Volume 1 | Number 1 | Jan 2013 | Pages 1–100

PCCP

Physical Chemistry Chemical Physics
www.rsc.org/pccp

ROYAL SOCIETY OF CHEMISTRY

This is an *Accepted Manuscript*, which has been through the Royal Society of Chemistry peer review process and has been accepted for publication.

Accepted Manuscripts are published online shortly after acceptance, before technical editing, formatting and proof reading. Using this free service, authors can make their results available to the community, in citable form, before we publish the edited article. We will replace this *Accepted Manuscript* with the edited and formatted *Advance Article* as soon as it is available.

You can find more information about *Accepted Manuscripts* in the Information for Authors.

Please note that technical editing may introduce minor changes to the text and/or graphics, which may alter content. The journal's standard Terms & Conditions and the Ethical guidelines still apply. In no event shall the Royal Society of Chemistry be held responsible for any errors or omissions in this *Accepted Manuscript* or any consequences arising from the use of any information it contains.

ROYAL SOCIETY OF CHEMISTRY

www.rsc.org/pccp
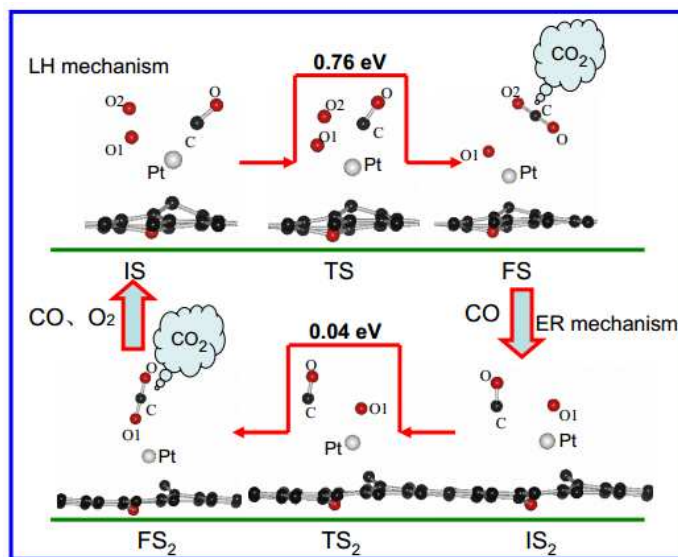
The oxidized graphene as the reactive support can control the stability and reactivity of single-atom Pt catalyst for CO oxidation.

Formation and Catalytic activity of Pt supported on oxidized graphene for CO oxidation reaction

Yanan Tang [a,b*], Xianqi Dai [a,b], Zongxian Yang [b], Lijun Pan [a], Weiguang Chen [a],

Dongwei Ma [c] and Zhansheng Lu [b]

[a] Department of Physics and Electronic Science, Zhengzhou Normal University,

Zhengzhou, Henan, 450044, People's Republic of China

[b] College of Physics and Electronic Engineering, Henan Normal University, Xinxiang,

Henan, 453007, People's Republic of China

[c] College of Physics and Electrical Engineering, Anyang Normal University, Anyang,

Henan, 455000, People's Republic of China

Abstract

The geometries, stabilities, electronic properties and catalytic capability of the platinum catalyst supported on oxidized graphene (Pt/OG) are investigated using the first-principles density-functional theory. Compared with the oxygen adatom, the hydroxyl molecule weakly adsorbs and easily aggregates on graphene, while the single oxygen adatom will form the epoxy group (EG) on pristine graphene or the oxygen dopant (OD) in defective graphene. The formation of EG and OD are used to model oxidized graphene (OG). The OD at the vacancy site forms the most stable configuration with small formation energy and large diffusion barrier, indicating that the OD is easier to incorporate into the graphene sheet. The OD sheet as substrate can effectively enhance the stability of Pt catalyst as compared with pristine graphene or

---
[*] Corresponding author. Tel/Fax: +86 371 65501661. E-mail address: yntang2010@hotmail.com (Y. Tang);

the grapheme sheet with EG. Moreover, the complete CO oxidation reactions on the Pt/OD system include a two-step process with the Langmuir-Hinshelwood (LH) reaction as a starting step followed by an Eley-Rideal (ER) reaction. The results suggest that the OD sheet can be used as the reactive support to control the stability and reactivity of catalysts, which opens up a new avenue for fabricating low cost and high efficient graphene-based catalyst.

1. Introduction

The catalytic oxidation of CO is becoming increasingly significant in the context of air cleaning and automotive emissions control.[1, 2] The use of catalysts activates the reaction between the reactants (O_2 and CO molecules) to remove the toxic CO.[3] To efficiently use the catalytic active components, it is expected that the catalysts are finely dispersed on the ideal support, which can not only enhance active area, but also reduce its consumption and cost. As a novel form of carbon-based substrate, graphene is a two-dimensional (2D) nanomaterial consisting of sp^2-hybridized carbon atoms arranged in a hexagonal lattice.[4] Owing to its unique structure, mechanical, thermal and electronic properties,[5-7] especially, the huge surface-to-volume ratio, graphene can serve as a support for catalytic nanoparticles.[8-10]

Graphene oxide (GO), one of the derivates of graphene, can be obtained through the chemical exfoliation of graphite.[11, 12] With respect to its structure, the studies assumed the presence of various oxygen functional groups on the GO.[13-16] The oxygen functional groups have been identified mainly in the form of hydroxyl (-OH) and epoxy groups on the basal plane.[17] However, the detailed analysis of the atomic structure and chemical activity for GO is lacking. Experimental results indicate that the highly reduced graphene oxide (RGO) primarily distributes oxygen containing groups.[18, 19] Besides, structural defects do exist in graphene,[20] which can be easily oxidized and terminated by oxygen adatom (forming epoxy group (EG) on pristine graphene or oxygen dopant (OD) in defective graphene).[21] For coverage less than 25%, the chemisorption energy of the hydroxyl groups turns out to be lower than that

3

of the oxygen atoms.[17] Furthermore, the hydroxyl groups can easily diffuse and lead

to the reaction with each other.[22] Recently, the theoretical studies predicted that the

GO structures with pure oxygen and C are energetically favored under high oxygen

chemical potential.[23] Therefore, the current study choose the GO structure model

including the formation of EG and OD on graphene sheet, and without taking into

account the coadsorption of hydroxyl groups and EG (or OG). Here, the simplistic

structure of GO sheet is viewed as the oxidized graphene (OG, including the structure

of EG or OD), which is in accordance with the structure proposed by Hofmann and

Holst.[24] The OG structure is different from the pristine graphene (pri-graphene) due to

the existence of carbon-oxygen bonds,[14, 25-28] which has wide applications in

electronics, sensor, and catalytic reaction.[29-31]

As known, the high price and the poor utilization rate of platinum (Pt) catalysts

limit its practical application. Thus reducing the particles size is one of the important

ways to lower the price and enhance the performance of catalyst. Experimental[32]

observations demonstrate that the nanosize Pt clusters on graphene have the high

catalytic performances, and the sub-nano-Pt clusters exhibit high CO tolerant on

graphene nanosheets.[33, 34] Due to the strong sp^2 bonds between carbon atoms in

graphene sheet, there are rather weak interaction between pri-graphene and the

supported metal atoms or clusters. This weak interaction may causes the Pt atoms

accumulation into larger structures on graphene and become less catalytically efficient.

Therefore, it is highly desirable for exploring an effective approach to improve the

stability and efficiency of catalyst.

4

The dopant in defect can modify the local curvature and electronic charge distribution, and consequently alter the chemical properties of the original carbon material.[35, 36] Recently, several studies observed that the metal atoms embedded graphene can enhance the adsorption of gas molecules [37-40]. Besides, some non-metal atoms doped graphene can improve the durability of a single-atom Pt catalyst,[41, 42] which is effective for catalyzing CO oxidation.[43] Theoretically, it is found that the single Pt-[44], Au-[45], Fe-[46] or Cu-[47] atoms in the defect graphene with single vacancy (SV-graphene) show high chemical activity for CO oxidation. The experimental result shows that a single-atom Pt uniformly dispersed on FeO_x and exhibited the excellent catalytic activity.[48] Meanwhile, the strong binding strength of Fe anchored on GO sheet also exhibits good catalytic activity,[49] where the O atoms on the surface can serve as the reactive sites to anchor metal atoms, which can be useful for exploring the reactivity of single-atom catalyst. These results mean that the single-atom catalyst on suitable substrate has important reference for validating the reactivity of catalysts in atomic-scale. Hence, we choose a single Pt atom anchored on the GO sheet for the study.

In general, the bare defective sites in graphene are always terminated by the oxygen atoms and may appear passivated or saturated, yet these oxygen-saturated vacancies sites are less reactive than the bare vacancies but considerably more reactive than the graphene.[21] However, there is a lack of understanding on how the formation process of oxygen atom adsorption on graphene (including the EG and OD) is, and how the oxygen-containing groups have effect on the catalyst durability and

chemical activity. Moreover, it remains unclear whether a single Pt atom can be catalytically active or have better performance on OG sheet than that on the pri-graphene (or SV-graphene).[44] Since the CO oxidation reaction is important in chemical engineering and nanocatalysis, we choose the prototype reaction on OG substrate as a reference to evaluate the reactivity of single-atom Pt catalyst.

In this paper, the adsorption and diffusion of oxygen atoms and hydroxyl groups on graphene substrate are comparatively studied. The hydroxyl group on pri-graphene has lower stability compared with the epoxy group, thus the high mobility of hydroxyl groups can easily react with each other. Besides, the single oxygen atom can form the EG on pri-graphene and the OD on SV-graphene, respectively. The formation of EG or OD on graphene can construct the structure of OG sheet. Compared with the EG, the OD is more suitable as a reactive substrate to anchor the Pt catalyst (Pt/OD). Moreover, the catalytic processes of CO oxidation on the Pt/OD are also studied through comparing the Langmuir-Hinshelwood (LH) and Eley-Rideal (ER) reactions. It is found that the LH reaction of CO and O_2 on the Pt/OD has smaller energy barrier than that of the ER reaction, thus the LH reaction as the first step followed by the ER reaction is the favorable mechanism. The results show that OD can serve as a good candidate for designing novel efficient graphene-based catalyst, which suggests a great potential for further application with the low-cost and high-activity.

2. Theoretical method and models

The spin-polarized density function theory (DFT) calculations are performed using the Vienna ab-initio simulation package (VASP).[50, 51] For improving the

calculation efficiency, core electrons are replaced by the projector augmented wave (PAW) pseudopotentials[52] and the generalized gradient approximation of Perdew, Burke, and Ernzernhof (PBE)[53] is used for exchange and correlation. The electrons of the C$2s2p$, O$2s2p$ and Pt $5d6s$ states are treated explicitly as valence electrons. The graphene sheet is represented using a hexagonal supercell containing 32 carbon atoms with a p (4×4) structure in the x-y plane. The distance between the graphene sheet and its images is set to 15 Å, which leads to negligible interactions between the systems and their mirror images. An energy cutoff of 400 eV is used for the plane wave expansion and the convergence criterion for the electronic self-consistent iteration is set to 10^{-5} eV. The Brillouin zone (BZ) integration is sampled using a 3×3×1 Γ-centered Monkhorst-Pack (MP) grid and a Γ-centered MP grid of 10×10×1 is used for the final density of states (DOS) calculations.

The calculated lattice constant of graphene is 2.47 Å, which is slightly larger than the experimental value of 2.46 Å.[54] The optimized C-C bonds are 1.43 Å. The graphene supercell is then built based on the calculated lattice constant. In the calculations, all the C atoms and adsorbate are allowed to relax in all directions. Bader charge analysis[55] is used to evaluate the electronic charge transfer in the reactions. The climbing image nudged elastic band method (CI-NEB)[56-58] is employed to investigate the saddle points and minimum energy paths (MEP) for the diffusion and dissociation of reactant gas molecules on Pt/OD surface. The optimized states and the transition states are tested by means of frequency calculations. According to the frequency calculations, the structures with no imaginary frequency correspond to the

stable configurations which can be chosen as the initial state (IS) and final state (FS) in the chemical reactions, while those with one imaginary frequency correspond to the metastable states which can be viewed as the intermediate states (MS). Four to eight images are inserted between the IS and FS, and the spring force between adjacent images is set to 5.0 eV Å^{-1}. Images are optimized until the forces on each atom are less than 0.02 eV Å^{-1}. Besides, the energy of an isolated atom is simulated using a cubic cell of $15 \times 15 \times 15$ Å^3 with oxygen, a platinum atom or a hydroxyl molecule. A single oxygen atom (or hydroxyl molecule) is placed on the surface at high symmetry positions over a carbon atom (T, the top site), the center of a carbon-carbon bond (B, the bridge site), or the center of a hexagon (H, the hollow site) on the pri-graphene as shown in Fig. 1(a). The oxygen dopant in graphene is represented by substituting a single oxygen atom into the carbon lattice. A Pt atom is placed and optimized at various test adsorption sites near the EG and OD (including the top site of O and its neighboring C atoms or the bridge sites of O-C and C-C bonds) to obtain the most stable configuration of the Pt/OG.

The adsorption energy (E_{ads}) is computed using the expression,

$$E_{ads} = E_A + E_B - E_{AB} \tag{1},$$

where E_A represents the total energy of adsorbate A (e.g., a single oxygen atom, a hydroxyl molecule, a Pt atom or a free gas molecule of O_2, CO or CO_2); E_B represents the total energy of substrate B (e.g., the pri-graphene, SV-graphene, OD or Pt/OD), and E_{AB} represents the total energy of system.

The formation energy ($\triangle E$) of a oxygen dopant is given by the formula:

$$\Delta E = E_{gra+O} + E_C - E_{pri+O} \qquad (2),$$

where E_{gra+O} is the total energy of the graphene with an oxygen dopant; E_{pri+O} is the total energy of the pri-graphene with an oxygen adatom, and E_C is the energy of a C atom in the pri-graphene.

3. Results and discussion

3.1 Adsorption energy and stable geometry

Firstly, the adsorptions of an oxygen atom or a hydroxyl molecule on the basal plane of pri-graphene and SV-graphene sheets are studied. The adsorption energies (E_{ads}), transferred electrons (Δq) and the bond lengths are shown in Table 1. On pri-graphene, the most favorable adsorption for a single O atom is found to occur at the bridge site of C-C bond (E_{ads} = 2.42 eV) and the C-O bond length is 1.47 Å, as shown in Fig. 1(b). The two carbon atoms bound with the O atom are pulled out of the graphene plane by 0.32 Å, which is in agreement with previous calculations.[59-63] The adsorbed O atom makes C-C bond expands from 1.41 Å in graphene to 1.50 Å, which is close to the sp^3 bond lengths (1.54 Å) in diamond. Such bond expansion in the presence of oxygen has been previously predicted for epoxy groups (EG) on pri-graphene.[19, 64] As shown in Fig. 1(c), the hydroxyl molecule is placed at the top site of C atom on pri-graphene, the calculated E_{ads} is 0.57 eV and the corresponding O-H bond length is 0.98 Å. The adsorbed hydroxyl group causes the carbon atom pulled out by 0.50 Å, inducing local structural distortions on the graphene surface. The adsorbed hydroxyl molecule breaks one of the C-C π bonds and transforms the sp^2 hybridization to the sp^3. Therefore, the sp^3-like bonding characters for the stable

9

configuration mainly come from the geometrical constraints.

On the SV-graphene, an oxygen atom or a hydroxyl molecule is placed at the center of defective site, the top of different carbon atoms (C_n for n=1, 2 and 3), or the bridge sites as shown in Fig. 1(a). It is found that the O adatom adsorbed at the SV and C_1 sites have much larger adsorption energies (8.35 and 6.61 eV) as compared with that of hydroxyl molecule (2.81 and 3.85 eV). The O adatom is considerable unstable at the bridge site of C_1-C_2 bond, where the O atom is finally trapped at the C_1 site. The O adatom adsorbed at the bridge sites of C_2-C_3 has an E_{ads} of 2.54 eV, which is slightly larger than that on the pri-graphene. In comparison, the hydroxyl molecule is placed at the top sites of C_2 and C_3 with the small E_{ads} of 0.91 and 1.46 eV, respectively. The local curvature of graphene is pulled out by the adsorbed epoxy or hydroxyl group, which make the graphene sheet transform from a plane sp^2-like hybridized to a distorted sp^3-like hybridized geometry. In a word, the oxygen atom and hydroxyl molecule adsorbed near the vacancy sites form the more stable configurations than those on the pri-graphene. In addition, the epoxy and hydroxyl groups can serve as electrons acceptor since the oxygen atom has stronger electronegativity than that of the carbon atom, as shown in Table 1. Compared with the metal dopant,[65] the O dopant in graphene has the smaller formation energy (1.96 eV), indicating that the oxygen atom is easier to be incorporated into the defective site to form the OD sheet.

In general, the diffusion barriers would illustrate the weak or strong interaction between the substrate and the adsorbate. The previous results[46, 65-68] show that the

10

adatoms on pri-graphene has smaller diffusion barriers as compared with that on SV-graphene. NEB calculations show that individual OH could easily diffuse on pri-graphene surface with small energy barrier 0.35 eV along a pathway between equilibrium states (from one top site of carbon atom to the next one). In contrast, the O adatom has larger diffusion barrier (0.73 eV) from a bridge site to a neighboring bridge site and the nearest top site of C atom is considered as transition state (TS). which is in accordance with the previous result.[69] Besides, the trapped O adatom needs larger energy to break away from SV to C_1 site (2.26 eV) and then diffuses from C_1 site to the bridge of C_2-C_3 (4.8 eV). The larger energy barriers suggest that the O adatom is quite immobile at the defective site on graphene, yet the high mobile hydroxyl group could easily rotate or diffuse on graphene surface, so it tends to aggregate and reacts with another hydroxyl group to form the water molecule[22] and leave the EG (or OD) on graphene sheet. In the following sections, we show that the OG sheet (including the EG or OD on graphene) can be used as the reactive surface to control the stability of supported Pt catalyst.

3.2. The adsorption of gas molecules on the Pt/OD sheet

The supported Pt catalyst on OG sheet (denotes as Pt/OG) is modeled with a single Pt atom anchored on the EG and OD sheets, respectively. The most stable configuration of the Pt atom is sought by comparing the optimizing structures with various possible adsorption sites. Fig. 2(a) shows the most stable geometric structure of the optimized Pt/OD system, which is in agreement with the results demonstrated by Groves et al.[41] One of the O-C bond breaks and the Pt atom interacts with the

dangling sp^2 bond of carbon atom at the defective site. The adsorption height (h) of the Pt adatom is 2.51 Å above the surface. The O dopant is pushed out by 0.43 Å below the surface plane and binds to two carbon atoms forming a C-O-C structure. The Pt-C bond is 1.85 Å and the C atom is drawn out 0.87 Å by the binding of Pt atom. It is found that the adsorption of Pt on the OD sheet has much higher stability (E_{ads} = 3.38 eV) as compared with those on the pri-graphene (E_{ads} =1.55 eV). At sites nearby of the epoxy group, including the top site of O atom, the first nearest neighboring B site, second neighboring B site and third neighboring B site of C-C bonds, the corresponding adsorption energies vary from 1.23 to 1.37 eV. Thus the stability of Pt catalyst is greatly improved on the OD surface. Although the amounts of epoxy groups on GO sheets may be more than those of the O dopants in graphene, the OD sheet as the reactive support can improve the dispersion of the supported catalysts. In the later section, we will mainly discuss the adsorptive stability and electronic structure of gas molecules (CO and O_2) on the Pt/OD substrate.

To gain more insight into the origin of the high stability of the Pt/OD systems, we investigate the electronic density of states (DOS) plots as shown in Fig. 3, which includes the total DOS (TDOS) of the SV-graphene and OD systems. The SV-graphene exhibits magnetic character with the DOS plots of the spin-up and spin-down channels unsymmetric. A sharp peak situates at the Fermi level (E_F), which mainly originates from the dangling-bond states of the undercoordinated carbon atoms around the vacancy. However, the peaks at the Fermi level in the DOS plots of the OD system decrease due to the partially saturation of the dangling-bonds by the oxygen

dopant. The DOS plots of the spin-up and spin-down channels become symmetric, suggesting that the system is nonmagnetic. Moreover, the OD states have been strongly altered with the adsorption of Pt atom. The peaks at the Fermi level disappear and strong hybridization between Pt $5d$ states and carbon atom $2p$ states can be seen both above and below the Fermi level. This indicates that the Pt $5d$ states play an important role to enhance the interaction with the dangling bonds of carbon atoms at the defect site of graphene.

Herein, we study the adsorption of CO and O_2 on the Pt/OD substrate. The most energetically favorable configuration of O_2 on the Pt/OD is shown in Fig. 2(b), which is characterized by the O-O bond paralleling to the graphene surface forming two chemical bonds with Pt atom, and the calculated E_{ads} is 0.96 eV. About 0.5 electrons are transferred from the Pt/OD to O_2, which occupy the antibonding $2\pi^*$ states of O_2 and subsequently lead to the elongation of the O-O bond from 1.23 to 1.36 Å. As shown in Fig. 4(a), the partial DOS (PDOS) peaks of Pt are narrow and sharp before the adsorption of O_2. In comparison, the PDOS peaks of Pt $5d$ states are strongly altered when O_2 is adsorbed. The broadened and reduced peak of Pt $5d$ states is due to the hybridization of the transferred electrons with the O_2 $2\pi^*$ and 5σ states around the E_F. The hybridization between the adsorbed O_2 and Pt induces the magnetic moment (2.0 μ_B) of whole system due to the increase of unpaired electron number, which is similar to that on the Au-[45] and Cu-graphene system.[47]

The CO adsorbs on the Pt/OD system with an end-on configuration as shown in Fig. 2(c). The C-O bond length is elongated (1.17 Å) as compared with that of the free

CO molecule (1.14 Å). The calculated adsorption energy of CO (1.77 eV) is larger than that of O_2. The strong hybridization between Pt *6s*, *5d* and CO *2π** states near the E_F is observed, as shown in Fig. 4(b). Compared with the bare Pt/OD system, the slightly increased of Pt *5d* peaks move near to the E_F in the CO adsorbed Pt/OD substrate due to the transferring of electrons from the *5σ* states to Pt atom. Meanwhile, the charge transfer occurs from the occupied Pt *5d* states to the CO *2π** states, which is responsible for the strong CO-metal binding. The adsorption of CO does not change the magnetic moment of the whole system (zero $μ_B$). In contrast, the adsorption of O_2 induces dramatic changes on electronic structure and localized spin polarization of Pt/OD substrate. The analysis of DOS plots shows that the main contribution of the hybridization comes from the O_2 *2π**, *5σ* orbitals (CO *2π** orbitals) and Pt *5d* orbitals. Hence, the above results indicate that one can control the electronic properties and spin polarization of a system in graphene engineering through using appropriate adsorbate.

Electronic structures play a fundamental role in the physical and chemical properties. Therefore, we calculated the charge density difference (CDD) of the optimized configurations for the system with the gas molecules (CO and O_2) on the Pt/OD. The results are depicted in Figure 5, in which the contour lines in plots are drawn at 0.03 e/Å^3 intervals. In Pt/OD system, unlike the carbon atom in graphene that binds with three carbon atoms to form the sp^2 hybridization, the compressed O atom binds with two dangling bonds of carbon atoms and gains 1.50 electrons, while the adsorbed Pt atom binds with the rest sp^2 dangling bond of carbon atom and gains

0.09 electrons. The CDD in Figs. 5(a)-(b) suggests the charge redistribution due to the adsorption of O_2 (or CO) on the Pt/OD substrate, where the solid (dashed) lines denote the charge accumulation (depletion). It is found that the electrons deplete from the vicinity of the Pt atoms and accumulate in the vicinity of the $Pt-O_2$ or the CO-Pt interfaces. Bader charge analysis[55] shows that the adsorbed CO and O_2 gain about 0.26 and 0.50 electrons, and the Pt atoms lose about 0.27 and 0.52 electrons, respectively, indicating that the gaining electrons of the adsorbate mainly come from the Pt atom. Compared with the adsorption energies of CO (2.84 eV) and O_2 (1.39 eV) on the Pt/pri-graphene,[44] the CO (1.77 eV) and O_2 (0.96 eV) on the Pt/OD system have smaller adsorption energies, because the adsorbed gas molecules (CO, 0.26 e and O_2, 0.50 e) gain less electronic charge from the Pt atom in Pt/OD substrate than those on the Pt/pri-graphene (CO, 0.30 e and O_2, 0.60 e). Besides, the smaller (larger) charge density accumulation between the CO (O_2) and Pt/OD substrates indicates that the adsorbed O_2 gains more electrons and exhibits stronger ability as electron-acceptor than does the CO molecule.

The coadsorption of CO and O_2 molecules on the Pt/OD substrate is also studied. The computations reveal that the coadsorption CO and O_2 has larger E_{ads} of 2.28 eV than the individual E_{ads} values of CO and O_2 molecules. It is found that the coadsorption energy of CO and O_2 is larger than that of the E_{ads} value of CO (1.77 eV), indicating that E_{ads} of O_2 on CO preadsorbed Pt/OD is 0.51 eV, thus the O_2 prefers to adsorb and react with CO, which enhances the reaction possibility for $CO+O_2$ reaction. In addition, we test two CO (or two O_2) molecules adsorption on the Pt/OD and the

corresponding adsorption energy is reduced to 1.12 eV (or 0.88 eV), respectively. This result indicates that the stability of adsorptive CO is more easily affected in gas environment compared with that of O_2 molecule. Besides, the CO_2 molecule has a much smaller E_{ads} (0.21 eV) on the Pt/OD, suggesting that a CO_2 molecule can easily desorbs from the reaction site at room temperature due to the weak adsorption.

3.3. The catalytic oxidation of CO on Pt/OD system

There are two well-known mechanisms for the catalytic reaction of O_2 with CO, namely the Langmuir-Hinshelwood (LH) and the Eley-Rideal (ER) mechanism.[70, 71] The LH mechanism involves the coadsorption of O_2 and CO molecules before reaction, the formation of an intermediate state and desorption of CO_2 molecule. In the ER mechanism, the preadsorbed O_2 reacts directly with the physisorbed CO molecule. The adsorptive ability of gas molecule determines the reaction pathways on the catalyst. The above results demonstrate that the adsorption energies of gas molecules are greatly decreased when the more molecules adsorb on Pt catalyst, and the coadsorption of CO and O_2 has the moderate adsorption energy on the Pt/OD substrate, thus we will mainly discuss the LH reaction for CO oxidation.

To have a better understanding on the LH mechanism, the coadsorption of CO and O_2 on the Pt/OD is studied, as shown in Fig. 6(a). In the optimized structure, the distance between CO and O_2 molecules is 3.28 Å with the CO-Pt and O_2-Pt distances of 1.88 Å and 2.68 Å, respectively. The structural parameters of the states along the MEP for the CO oxidation are shown in Table 2. In the reaction pathway, one of the oxygen atoms in the O_2 molecule starts to approach the carbon atom of CO to reach

the TS (a peroxo-type O-O-C-O complex with an energy barrier of 0.76 eV), where

the O-O bond of O_2 is elongated to 1.38 Å. Passing over the TS, the O-O bond is

continually elongated without any energy barrier and a physisorbed CO_2 is formed,

leaving an atomic oxygen (O_{ads}) on the Pt atom. After the release of the CO_2 molecule,

we further check the oxidation process of a second CO with the atomic O_{ads} by the ER

reaction. The structure with preadsorbed O_{ads} and a subsequent CO near the Pt atom is

considered as the IS. The distance between O-Pt is 1.82 Å, and the CO molecule is

placed away from the atomic O_{ads} (2.95 Å). The FS is simply chosen as the

configuration of CO_2 adsorbs on the Pt/OD, as shown in Fig. 6(b). The reaction has a

very small energy barrier (0.04 eV), suggesting that the atomic O_{ads} is very active for

CO oxidation. In contrast to the energy barriers of CO oxidation reaction by the LH

process (CO+O_2→OOCO→CO_2+O_{ads}) on Au-graphene (0.31 eV) and Cu-graphene

(0.54 eV) systems,[45, 47] the formation of first CO_2 on the Pt/OD has a relatively larger

energy barrier (0.76 eV). However, the formation of second CO_2 through the ER

process (CO+O_{ads}→CO_2) has a much smaller energy barrier (0.04 eV) as compared

with those on the Au-graphene (0.18 eV),[45] the Pt/FeO$_x$ (0.79 eV)[48] and the

Fe/graphene oxide (0.93 eV).[49] In addition, it was found that the formed of O-O-C-O

complex is as a metastable state on the Cu-graphene, while the O-O-C-O complex on

Pt/OD substrate appears as a transition state. Overall, the complete CO oxidation

reactions (including LH reaction, CO+O_2→OOCO→CO_2+O_{ads} and ER reaction,

CO+O_{ads}→CO_2) have modest energy barrier on the Pt/OD substrate, which is slightly

smaller than that on the Pt/pri-graphene,[44] thus the Pt/OD can be used as the reactive

surface to facilitate the catalytic cycle of CO oxidation reactions.

On the other hand, as an important reference, the ER reaction process as the starting reaction for CO oxidation with preadsorbed O_2 molecule on the Pt/OD is also studied. The reaction states along the MEP are shown in Fig. 6(c). The optimized configuration of CO above the preadsorbed O_2 on the Pt/OD is selected as the IS. The CO molecule approaches the activated O_2, and inserts into the O-O bond forming a carbonate-like intermediated state CO_3. This process overcomes an energy barrier of 0.83 eV due to the breaking of the O-O bond and the formation of the new C-O bonds. The same process with carbonate-like state CO_3 formation is also observed in the oxidation reactions on the Fe-embedded graphene [46] and the Fe-anchored graphene oxide.[49] The formed CO_3 is quite stable which needs to overcome a large energy barrier of 1.28 eV (at TS2) to produce a CO_2. Once formed, the produced CO_2 molecule may desorbs easily, leaving an atomic O_{ads} binding with Pt in the FS. Obviously, the energy barriers of the ER reaction for CO oxidation are larger than those of the LH reaction. Besides, considering that the adsorption energy of an individual CO molecule on Pt/OD substrate is larger than that of the O_2, and the intermediate state CO_3 is more stable than the final state (a free CO_2 and an O_{ads}), the system may be trapped at the CO_3 state, thus the ER reaction is impossible to be the starting state for the CO oxidation reaction. Instead, the LH reaction as the starting state is energetically more favorable on Pt/OD substrate.

Based on the above discussions, the two-step reaction for the CO oxidation has the modest energy barriers on the Pt/OD substrate. Compared with the ER reaction,

the LH reaction as a starting step is the energetically favorable mechanism, which ensures the high efficiency in the catalytic CO oxidation process. The coadsorption of CO and O_2 forms the OOCO complex, which easily dissociates into a CO_2 and an atomic O_{ads}. Therefore, the favorable pathway for CO oxidation starts with the LH reaction $(CO+O_2 \rightarrow OOCO \rightarrow CO_2+O_{ads})$ followed with an ER process $(CO+O_{ads} \rightarrow CO_2)$. Besides, the CO oxidation in the followed ER reaction step has a much smaller energy barrier than that of the first step of LH reaction, indicating that the energy barrier mainly comes from the formation of OOCO state. The Pt/OD system would be a good candidate catalyst based on graphene sheet with lower cost and higher activity for CO oxidation, which validates the reactivity of catalysts in atomic-scale.

4. Conclusion

In this paper, we model a good catalyst that consists of the single-atom Pt atom anchored on the OD substrate. The large pucker and charge redistribution around the vacancy zone can enhance the stability of oxygen adatom and hydroxyl molecule. In contrast to the oxygen adatom, the smaller diffusion barrier of hydroxyl group on graphene indicates that these adatoms can easily aggregate and react with each other. The single oxygen adatom can form the EG on the pri-graphene and the OD on the SV-graphene, and the formation of EG or OD on graphene can construct the structure of OG sheet. Compared with the EG, the OD is more suitable as a reactive substrate to anchor the Pt catalyst (Pt/OD). Moreover, it is found that the first step of CO oxidation through ER reaction has larger energy barrier than that of the LH reaction.

Then the second CO molecule (ER reaction) can be easily oxidized by the atomic O_{ads} on the Pt catalyst, and the corresponding energy barrier is much smaller than that of the first LH reaction. The results show that the Pt/OD system exhibits high catalytic activity for CO oxidation. This work would provide beneficial reference to stimulate the applications of graphene-metal nanocomposites catalysis in energy-related devices, and improve the efficiency, stability and cost-effectiveness of carbon-based materials.

References:

1 M. Shelef and R. W. McCabe, *Catal. Today*, 2000, **62**, 35-50.

2 M. V. Twigg, *Appl. Catal. B: Environ.*, 2007, **70**, 2-15.

3 M. S. Chen, Y. Cai, Z. Yan, K. K. Gath, S. Axnanda and D. W. Goodman, *Surf. Sci.*, 2007, **601**, 5326-5331.

4 A. K. Geim and K. S. Novoselov, *Nat. Mater.*, 2007, **6**, 183-191.

5 M. Orlita, C. Faugeras, P. Plochocka, P. Neugebauer, G. Martinez, D. K. Maude, A. L. Barra, M. Sprinkle, C. Berger, W. A. de Heer and M. Potemski, *Phys. Rev. Lett.*, 2008, **101**, 267601.

6 C. G. Lee, X. D. Wei, J. W. Kysar and J. Hone, *Science*, 2008, **321**, 385.

7 A. A. Balandin, S. Ghosh, W. Bao, I. Calizo, D. Teweldebrhan, F. Miao and C. N. Lau, *Nano Lett.*, 2008, **8**, 902-907.

8 G. Williams, B. Seger and P. V. Kamat, *ACS Nano*, 2008, **2**, 1487-1491.

9 G. M. Scheuermann, L. Rumi, P. Steurer, W. Bannwarth and R. Mulhaupt, *J. Am. Chem. Soc.*, 2009, **131**, 8262-8270.

10 B. Seger and P. V. Kamat, *J. Phys. Chem. C*, 2009, **113**, 7990-7995.

11 W. H. Zhang, V. Carravetta, Z. Li, Y. Luo and J. L. Yang, *J. Chem. Phys.*, 2009, **131**, 244505.

12 K. Erickson, R. Erni, Z. Lee, N. Alem, W. Gannett and A. Zettl, *Adv. Mater.*, 2010, **22**, 4467-4472.

13 J. A. Yan, L. Xian and M. Chou, *Phys. Rev. Lett.*, 2009, **103**, 86802.

14 Z. Wei, D. E. Barlow and P. E. Sheehan, *Nano Lett.*, 2008, **8**, 3141-3145.

15 G. Eda and M. Chhowalla, *Adv. Mater.*, 2010, **22**, 2392-2415.

16 F. Kim, L. J. Cote and J. Huang, *Adv. Mater.*, 2010, **22**, 1954-1958.

17 D. W. Boukhvalov and M. I. Katsnelson, *J. Am. Chem. Soc.*, 2008, **130**, 10697-10701.

18 O. C. Compton, D. A. Dikin, K. W. Putz, L. C. Brinson and S. B. T. Nguyen, *Adv. Mater.*, 2010, **22**, 892-896.

19 H. C. Schniepp, J. L. Li, M. J. McAllister, H. Sai, M. Herrera-Alonso, D. H. Adamson, R. K. Prud'homme, R. Car, D. A. Saville and I. A. Aksay, *J. Phys. Chem. B*, 2006, **110**, 8535-8539.

20 F. Banhart, J. Kotakoski and A. V. Krasheninnikov, *ACS nano*, 2010, **5**, 26-41.

21 J. M. Carlsson, F. Hanke, S. Linic and M. Scheffler, *Phys. Rev. Lett.*, 2009, **102**, 166104.

22 N. Ghaderi and M. Peressi, *J. Phys. Chem. C*, 2010, **114**, 21625-21630.

23 L. Wang, Y. Y. Sun, K. Lee, D. West, Z. F. Chen, J. J. Zhao and S. B. Zhang, *Phys. Rev. B*, 2010, **82**, 161406.

24 D. R. Dreyer, S. Park, C. W. Bielawski and R. S. Ruoff, *Chem. Soc. Rev.*, 2010, **39**, 228-240.

25 V. C. Tung, M. J. Allen, Y. Yang and R. B. Kaner, *Nat. Nanotechnol.*, 2008, **4**, 25-29.

26 Z. S. Wu, W. Ren, L. Gao, J. Zhao, Z. Chen, B. Liu, D. Tang, B. Yu, C. Jiang and H. M. Cheng, *ACS nano*, 2009, **3**, 411-417.

27 C. Gómez-Navarro, R. T. Weitz, A. M. Bittner, M. Scolari, A. Mews, M. Burghard and K. Kern, *Nano Lett.*, 2007, **7**, 3499-3503.

28 D. Yang, A. Velamakanni, G. Bozoklu, S. Park, M. Stoller, R. D. Piner, S. Stankovich, I. Jung, D. A. Field and C. A. Ventrice Jr, *Carbon*, 2009, **47**, 145-152.

29 I. Lightcap, T. Kosel and P. Kamat, *Nano Lett.*, 2010, **10**, 577-583.

30 S. Stankovich, D. Dikin, G. Dommett, K. Kohlhaas, E. Zimney, E. Stach, R. Piner, S. Nguyen and R. Ruoff, *Nature*, 2006, **442**, 282-286.

31 W. Yang, K. R. Ratinac, S. P. Ringer, P. Thordarson, J. J. Gooding and F. Braet, *Angew. Chem. Int. Ed.*, 2010, **49**, 2114-2138.

32 E. Yoo, T. Okata, T. Akita, M. Kohyama, J. Nakamura and I. Honma, *Nano Lett.*, 2009, **9**, 2255-2259.

33 E. Yoo, T. Okada, T. Akita, M. Kohyama, I. Honma and J. Nakamura, *J. Power Sources*, 2011, **196**, 110-115.

34 Y. N. Tang, Z. X. Yang and X. Q. Dai, *J. Nanopart. Res.*, 2012, **14**, 844.

35 M. Wu, C. Cao and J. Z. Jiang, *Nanotechnology*, 2010, **21**, 505202.

36 K. Suggs, V. Person and X.-Q. Wang, *Nanoscale*, 2011, **3**, 2465-2468.

37 M. Zhou, Y. H. Lu, Y. Q. Cai, C. Zhang and Y. P. Feng, *Nanotechnology*, 2011, **22**, 385502.

38 J. Y. Dai and J. M. Yuan, *J. Phys: Condens. Matter*, 2010, **22**, 225501.

39 J. Y. Dai and J. M. Yuan, *Phys. Rev. B*, 2010, **81**, 165414.

40 J. Y. Dai, J. M. Yuan and P. Giannozzi, *Appl. Phys. Lett.*, 2009, **95**, 232105.

41 M. N. Groves, C. Malardier-Jugroot and M. Jugroot, *J. Phys. Chem. C*, 2012, **116**, 10548-10556.

42 M. N. Groves, A. S. W. Chan, C. Malardier-Jugroot and M. Jugroot, *Chem. Phys. Lett.*, 2009, **481**, 214-219.

43 Y. N. Tang, Z. X. Yang, X. Q. Dai, D. W. Ma and Z. M. Fu, *J. Phys. Chem. C*, 2013, **117**, 5258-5268.

44 Y. N.Tang, Z. X. Yang and X. Q. Dai, *Phys. Chem. Chem. Phys.*, 2012, **14**, 16566-16572.

45 Y. H. Lu, M. Zhou, C. Zhang and Y. P. Feng, *J. Phys. Chem. C*, 2009, **113**, 20156-20160.

46 Y. F. Li, Z. Zhou, G. T. Yu, W. Chen and Z. F. Chen, *J. Phys. Chem. C*, 2010, **114**, 6250-6254.

47 E. H. Song, Z. Wen and Q. Jiang, *J. Phys. Chem. C*, 2011, **115**, 3678-3683.

48 B. T. Qiao, A. Q. Wang, X. F. Yang, L. F. Allard, Z. Jiang, Y. T. Cui, J. Y. Liu, J. Li and T. Zhang, *Nat. Chem.*, 2011, **3**, 634-641.

49 F. Li, J. Zhao and Z. Chen, *J. Phys. Chem. C*, 2012, **116**, 2507-2514.

50 G. Kresse and J. Furthmüller, *Comput. Mater. Sci.*, 1996, **6**, 15-50.

51 G. Kresse and J. Furthmüller, *Phys. Rev. B*, 1996, **54**, 11169-11186.

52 G. Kresse and D. Joubert, *Phys. Rev. B*, 1999, **59**, 1758-1775.

53 J. P. Perdew, K. Burke and M. Ernzerhof, *Phys. Rev. Lett.*, 1996, **77**, 3865-3868.

54 J. M. Carlsson and M. Scheffler, *Phys. Rev. Lett.*, 2006, **96**, 46806.

55 G. Henkelman, A. Arnaldsson and H. Jónsson, *Comput. Mater. Sci.*, 2006, **36**, 354-360.

56 G. Henkelman, B. Uberuaga and H. Jónsson, *J. Chem. Phys.*, 2000, **113**, 9901-9904.

57 G. Henkelman and H. Jónsson, *J. Chem. Phys.*, 2000, **113**, 9978-9985.

58 T. Zhu, J. Li and S. Yip, *Phys. Rev. Lett.*, 2004, **93**, 25503.

59 S. P. Chan, G. Chen, X. Gong and Z. F. Liu, *Phys. Rev. Lett.*, 2003, **90**, 86403.

60 D. Lamoen and B. Persson, *J. Chem. Phys.*, 1998, **108**, 3332.

61 P. Giannozzi, R. Car and G. Scoles, *J. Chem. Phys.*, 2003, **118**, 1003.

62 K. A. Mkhoyan, A. W. Contryman, J. Silcox, D. A. Stewart, G. Eda, C. Mattevi, S. Miller and M. Chhowalla, *Nano Lett.*, 2009, **9**, 1058-1063.

63 J. A. Yan and M. Chou, *Phys. Rev. B*, 2010, **82**, 125403.

64 J. L. Li, K. N. Kudin, M. J. McAllister, R. K. Prud'homme, I. A. Aksay and R. Car, *Phys. Rev. Lett.*, 2006, **96**, 176101.

65 Y. N. Tang, Z. X. Yang and X. Q. Dai, *J. Chem. Phys.*, 2011, **135**, 224704.

66 Y. J. Gan, L. T. Sun and F. Banhart, *Small*, 2008, **4**, 587-591.

67 O. Cretu, A. V. Krasheninnikov, J. A. Rodríguez-Manzo, L. Sun, R. M. Nieminen and F. Banhart, *Phys. Rev. Lett.*, 2010, **105**, 196102.

68 S. Malola, H. Häkkinen and P. Koskinen, *Appl. Phys. Lett.*, 2009, **94**, 043106.

69 A. M. Suarez, L. R. Radovic, E. Bar-Ziv and J. O. Sofo, *Phys. Rev. Lett.*, 2011, **106**, 146802.

70 L. M. Molina and B. Hammer, *J. Catal.*, 2005, **233**, 399-404.

71 W. An, Y. Pei and X. C. Zeng, *Nano Lett.*, 2008, **8**, 195-202.

Table.1. The adsorption energy (E_{ads}, in eV), adsorption height (h, Å), C-C bond length (b_{C-C}, Å), O-H bond length (b_{OH}, Å), O-C bond length (b_{O-C}, Å), distance between OH and nearest C atom (b_{OH-C}, Å), height of the stretched C atom (z_C, Å), the number of electrons transferred from the graphene substrates to the adsorbates (Δq, e), for the oxygen and hydroxyl adatom on the pri-graphene and SV-graphene. The SV site is fixed at one site and the adsorbates are placed on the different sites (C_n for n=1, 2 and 3) of carbon atoms as shown in Fig.1.

Oxygen	E_{ads}	h	b_{C-C}	b_{O-C}	z_C	Δq
B	2.42	1.54	1.51	1.47	0.28	0.98
SV	8.35	0.25	1.39	1.50	0.07	1.23
C1	6.61	1.87	1.48	1.23	0.82	1.81
C2-C3	2.54	1.62	1.50	1.47-1.48	0.37	0.82
Hydroxyl	E_{ads}	b_{OH-C}	b_{C-C}	b_{OH}	z_C	Δq
T	0.57	1.51	1.50	0.98	0.50	0.47
SV	2.81	1.52	2.54	1.00	0.22	0.56
C1	3.85	1.35	1.42	0.98	0.80	0.95
C2	0.91	1.45	1.50	0.98	0.44	0.69
C3	1.46	1.48	1.50	0.98	0.47	0.57

Table.2. Structural parameters of the CO oxidation on the Pt/OD substrate at each states along the MEP, (a) the process of $CO+O_2\rightarrow OOCO\rightarrow CO_2+O_{ads}$, (b) $CO+O\rightarrow CO_2$, IS, TS and FS are displayed in Fig. 6(a)-(b); (c) the process of $CO+O_2\rightarrow CO_3\rightarrow CO_2+O_{ads}$, IS, TS, MS and FS are displayed in Fig. 6(c).

(a)	IS	TS	FS
d_{Pt-O1}	2.68	1.98	1.78
d_{O1-O2}	1.25	1.38	2.98
d_{C-O2}	3.37	1.83	1.18
d_{C-O}	1.16	1.18	1.18
d_{C-Pt}	1.89	2.06	3.48

(b)	IS	TS1	MS	TS2	FS
d_{O1-O2}	1.32	1.39	2.18	2.51	3.08
d_{C-O}	1.14	1.17	1.22	1.18	1.18
d_{C-O1}	3.13	2.59	1.32	1.21	1.18
d_{C-O2}	2.93	1.69	1.37	2.04	2.74
d_{O1-Pt}	2.19	1.98	2.08	2.42	3.34
d_{O2-Pt}	2.04	2.58	2.01	1.88	1.82

Figure captions

Figure 1: Schematic diagram illustrating (a) the three high symmetry sites: the hollow (*H*), the top (*T*) and the bridge (*B*) for adatom on graphene, (b) a single oxygen atom and (c) hydroxyl molecule adsorbs on graphene. The big and small white sphere denotes the single vacancy (SV) and hydrogen atom. The indices of the C atoms are shown in the graphene.

Figure 2: Optimized structured models (a) the Pt/OD system, (b) the O_2 and (c) the CO adsorbed on the Pt/OD. Red, black, and white balls represent O, C and Pt atoms, respectively.

Figure 3: Spin-resolved total DOS (TDOS) for the SV-graphene and O-graphene, as well as TDOS and partial DOS (PDOS) for the Pt/OD system (spin-up is labeled with ↑ and spin-down is labeled with ↓). The thin, thick and dashed lines represent the TDOS of SV-graphene, O-graphene and Pt/OD systems, respectively, while the dotted and dash dotted lines represent the PDOS of Pt *5d* and C *2p* states in the Pt/OD. The vertical dotted line denotes the Fermi level.

Figure 4: Spin-resolved TDOS, local DOS (LDOS) for (a) O_2 and (b) CO on the Pt/OD system. The thick line represent the TDOS of O_2 on the Pt/OD, the thin, dashed and dash dotted lines represent the PDOS of Pt *5d*, *6s* states of without (with) O_2 or CO adsorption, the dotted lines represent the LDOS of adsorbed O_2 or CO. The vertical dotted line denotes the Fermi level.

Figure 5: Valence charge density difference plots of the Pt/OD with the (a) O_2 and (b) CO adsorbate, respectively. Contour lines in plots are drawn at about 0.03 e/Å^3 intervals, and the solid (dashed) lines denote the charge accumulation (depletion).

Figure 6: Minimum energy profiles and the configuration of different states including the IS, TS, MS and FS for CO oxidation on Pt/OD substrate, (a) CO + O_2 with the LH reaction, (b) of CO + O_{ads} with the ER reaction and (c) CO + O_2 with the ER reaction. Red, black, and white balls represent O, C and Pt atoms, respectively.